


Possibilities for synthesis of new transfermium isotopes in multinucleon transfer reactions

Xiao Jun Bao (包小军) ^{*}

Department of Physics, Collaborative Innovation Center for Quantum Effects, and Key Laboratory of Low Dimensional Quantum Structures and Quantum Control of Ministry of Education, Hunan Normal University, Changsha 410081, People's Republic of China



(Received 27 June 2021; accepted 20 August 2021; published 3 September 2021)

Multinucleon transfer mechanisms near barrier collisions between very heavy nuclei are investigated in the framework of the improved dinuclear system model by considering the influence of orientation effects combined with statistical model code GEMINI++. Several transfer reactions for different actinide targets (^{238}U , ^{248}Cm , and ^{249}Cf) are studied in detail. One notices that the isotopic distributions of the above-target products decrease drastically by a factor of 10 per proton, which is moved from projectile to target. However, the calculated and measured results show that the larger production cross sections above targetlike fragments can be produced by using the heaviest available target. The predicted cross sections and excitation functions of the new transfermium isotopes may be useful for future experiments.

DOI: [10.1103/PhysRevC.104.034604](https://doi.org/10.1103/PhysRevC.104.034604)

I. INTRODUCTION

Production of neutron-rich nuclei using the multinucleon transfer process is one of the major aims of modern low energy heavy-ion nuclear physics [1–5]. Forty years ago there had been a great deal of interest based on multinucleon transfer (MNT) reactions with actinide targets to synthesize heavy and superheavy nuclei [6,7]. Experimental investigations into multinucleon transfer reactions of actinide targets ranging from U to Cf with various projectiles ranging from ^{18}O to ^{238}U have been carried out in the 1970s and early 1990s at energies near the Coulomb barriers [1,6–12].

Pioneer experiments have shown that multinucleon transfer reactions between very heavy nuclei $^{238}\text{U} + ^{238}\text{U}$ and $^{238}\text{U} + ^{248}\text{Cm}$ [6,7] may provide the possibility for the production of superheavy nuclei. For the above mentioned two reactions, nucleons can be transferred from the lighter to the heavier nucleus to form leadlike nuclei in the multinucleon rearrangement process. Lately, this type of multinucleon rearrangement is the so-called inverse quasifission [13]. The mechanism of strongly damped collisions between very heavy nuclei is of great current interest to synthesize heavy and superheavy nuclei. However, the measured production cross sections of the heavy fragments between very heavy nuclei were found to decrease very rapidly with increasing atomic number [6,7].

The lack of suitable nuclear reactions to produce new neutron-rich transfermium isotopes has long hindered the study of these nuclei. Up to now, only neutron-deficient isotopes for the transfermium nuclei have been synthesized using fusion evaporation reactions [14]. Recently, renewed interest in multinucleon transfer reactions with heavy ions

has arisen. On the one hand, there are the limitations of fusion evaporation and neutron capture reactions for production of neutron-rich transfermium isotopes [14–17]. On the other hand, the obtained results based on multidimensional Langevin equations are rather optimistic for the formation of primary and surviving isotopes of some transfermium elements in the reaction $^{238}\text{U} + ^{248}\text{Cm}$ [17,18].

The multinucleon transfer reaction is a very complicated process. Accurate calculation of nucleon transfer probability is challenging work because complex nonequilibrium dynamics are involved in collective motion coupled with nuclear intrinsic motion. In recent years, many approaches have been developed to shed light onto the multinucleon transfer mechanism in heavy-ion collisions near barrier energies [4,13,17,19–48]. However, no approach is currently predominant. Therefore, it remains difficult for both experimentalists and theorists to assess various models of multinucleon transfer reactions and their predictions.

For the above reasons, one notices that systematic calculations of the existing experimental data are helpful to reveal multinucleon transfer mechanisms. Systematic calculation should include the following three aspects. First, theoretical results correctly describe the magnitude and maxima of the observed transfer cross sections for a wide range of transfers for a specific reaction. Second, the production cross sections of the multinucleon transfer by using different targets ranging from Sn to Cf with various projectiles ranging from ^{32}S to ^{238}U have been carried out at energies near the Coulomb barriers, and the calculated results can well describe the experimental data. Finally, a favorable beam energy should be sought to produce new isotopes. That is because the final yield is a product of the survival probability and primary cross section.

The improved dinuclear system (DNS) model is one of them, in which we construct a new four-variable master equation (ME) so that the deformations as well as the nucleon

^{*}baoxiaojun@hunnu.edu.cn

transfer are viewed consistently governed by MEs in the potential energy surface of the system. The calculations of the evaporation residue cross section for the cold and hot fusion reactions leading to superheavy nuclei and the multinucleon transfer cross sections are in good agreement with available experimental data [49–53].

In this paper I adopted the improved DNS model + GEMINI++ for the description of MNT reactions with ^{136}Xe and ^{238}U bombarded actinide targets and for the prediction of the corresponding production cross sections. From the theoretical point of view, the Coulomb barrier and depth of the pocket of the nucleus-nucleus potential are different for collisions of the deformed target or/and projectile nucleus with different orientations. The aim of the present paper is to consider the influence of orientation effects on the production cross section in the improved DNS model. To demonstrate the accuracy of the developed approach and learn about the prospects of synthesizing superheavy isotopes in strongly damped collisions between very heavy nuclei, the reaction systems $^{238}\text{U} + ^{238}\text{U}$, $^{238}\text{U} + ^{248}\text{Cm}$, $^{136}\text{Xe} + ^{248}\text{Cm}$, and $^{136}\text{Xe} + ^{249}\text{Cf}$ are investigated and compared with experimental data, and the predicted cross sections and excitation functions in the $^{248}\text{Cm} + ^{249}\text{Cf}$ reaction for the yields of neutron-rich fermium isotopes may be useful for future experiments.

II. THEORETICAL FRAMEWORK

The transfer cross section of a primary product $\sigma_{Z_1, N_1}^{\text{pri}}(E_{\text{c.m.}})$ in the diffusive nucleon transfer reaction based on the present improved DNS model is written as a sum over all partial waves

J [47]:

$$\begin{aligned} \sigma_{Z_1, N_1}^{\text{pri}}(E_{\text{c.m.}}) &= \frac{\pi \hbar^2}{2\mu E_{\text{c.m.}}} \sum_J (2J+1) T(E_{\text{c.m.}}, J) \\ &\times \sum_{\beta_1} \sum_{\beta_2} \int_0^{\pi/2} \sin \theta_1 d\theta_1 \int_0^{\pi/2} \\ &\times P(Z_1, N_1, \beta_1, \beta_2, J, \theta_1, \theta_2, \tau_{\text{int}}) \sin \theta_2 d\theta_2 \end{aligned} \quad (1)$$

where the transfer cross sections are calculated from zero to grazing angular momentum. The grazing angular momentum J_{gr} can be expressed as

$$J_{\text{gr}} = 0.22 R_{\text{cont}} \{A_{\text{red}} [E_{\text{c.m.}} - V(R_{\text{cont}})]\}^{1/2} \quad (2)$$

where $V(R_{\text{cont}})$ denotes the interaction barrier at the interaction radius R_{cont} . A_{red} is reduced mass (see Ref. [51] for more details). The penetration coefficient $T(E_{\text{c.m.}}, J)$ is estimated to be 1 when the incident energy is higher than the nucleus-nucleus interaction energy in the contact point R_{cont} . Because of the disappearance of the Coulomb barrier for a sufficiently heavy system, the contact point where the nucleon transfer process takes places can be assumed by $R_{\text{cont}} = R_1 [1 + \beta_1 Y_{20}(\theta_1)] + R_2 [1 + \beta_2 Y_{20}(\theta_2)] + 0.5$ fm, with $R_i = 1.16 A_i^{1/3}$.

One assumes that the orientation effects in the potential energy surface can be easily considered for separated frozen nuclei. The multinucleon rearrangement processes between the interacting projectile and target are described as a diffusion process by numerically solving a set of four-variable MEs in the corresponding potential energy surface. For fixed values θ_1 and θ_2 , the probability distribution function in Eq. (1)— $P(Z_1, N_1, \beta_1, \beta_2, t)$ for fragment 1 with Z_1 , N_1 , β_1 , and β_2 at time t —is described by the following master equations [53]:

$$\begin{aligned} \frac{dP(Z_1, N_1, \beta_1, \beta_2, t)}{dt} &= \sum_{Z'_1} W_{Z_1, N_1, \beta_1, \beta_2; Z'_1, N_1, \beta_1, \beta_2}(t) [d_{Z_1, N_1, \beta_1, \beta_2} P(Z'_1, N_1, \beta_1, \beta_2, t) - d_{Z'_1, N_1, \beta_1, \beta_2} P(Z_1, N_1, \beta_1, \beta_2, t)] \\ &+ \sum_{N'_1} W_{Z_1, N_1, \beta_1, \beta_2; Z_1, N'_1, \beta_1, \beta_2}(t) [d_{Z_1, N_1, \beta_1, \beta_2} P(Z_1, N'_1, \beta_1, \beta_2, t) - d_{Z_1, N'_1, \beta_1, \beta_2} P(Z_1, N_1, \beta_1, \beta_2, t)] \\ &+ \sum_{\beta'_1} W_{N_1, Z_1, \beta_1, \beta_2; N_1, Z_1, \beta'_1, \beta_2}(t) [d_{Z_1, N_1, \beta_1, \beta_2} P(Z_1, N_1, \beta'_1, \beta_2, t) - d_{Z_1, N_1, \beta'_1, \beta_2} P(Z_1, N_1, \beta_1, \beta_2, t)], \\ &+ \sum_{\beta'_2} W_{N_1, Z_1, \beta_1, \beta_2; N_1, Z_1, \beta_1, \beta'_2}(t) [d_{Z_1, N_1, \beta_1, \beta_2} P(Z_1, N_1, \beta_1, \beta'_2, t) - d_{Z_1, N_1, \beta_1, \beta'_2} P(Z_1, N_1, \beta_1, \beta_2, t)], \end{aligned} \quad (3)$$

where $W_{Z_1, N_1, \beta_1, \beta_2; Z'_1, N_1, \beta_1, \beta_2}$ is the mean transition probability from channel $(Z'_1, N_1, \beta_1, \beta_2)$ to $(Z_1, N_1, \beta_1, \beta_2)$. $d_{N_1, Z_1, \beta_1, \beta_2}$ denotes microscopic dimensions corresponding to the macroscopic state $(N_1, Z_1, \beta_1, \beta_2)$. β_1 and β_2 denote quadrupole deformations of fragments; they are considered as two discrete variables, corresponding to the projectilelike and targetlike fragments (TLFs), respectively. The initial condition of Eq. (1) is $P(N_P, Z_P, \beta_P, \beta_T, t=0) = 1$, where N_P and Z_P are the neutron and proton number of the projectile, and

β_P and β_T are the ground state quadrupole deformations of the projectile and target in the injection channel. The interaction time in the dissipative process of two colliding nuclei is determined by using the deflection function method [54–56]. The mean transition probability and microscopic dimensions are related to the local excitation energy. See Refs. [50,51,53] for more details.

The above mentioned mean transition probability and microscopic dimensions are related to the local excitation energy

(see Refs. [50,51] for more details). The local excitation energy ε^* is defined as [49]

$$\varepsilon^*(J) = E_x(J, t) - [U(N_1, Z_1, N_2, Z_2, R_{\text{cont}}, \beta_1, \beta_2, J) - U(N_P, Z_P, N_T, Z_T, R_{\text{cont}}, \beta_{10}, \beta_{20}, J)], \quad (4)$$

where the first term denotes that the dissipation energy $E_x(J, t)$ is converted from the relative kinetic energy loss. The second term in Eq. (4) is the driving potential energy of the system for the nucleon transfer of the DNS:

$$\begin{aligned} U(N_1, Z_1, N_2, Z_2, R_{\text{cont}}, \beta_1, \beta_2, J) &= B(N_1, Z_1, \beta_1) + B(N_2, Z_2, \beta_2) \\ &+ V_{\text{CN}}(N_1, Z_1, N_2, Z_2, R_{\text{cont}}, \beta_1, \beta_2) \\ &+ V_{\text{rot}}(N_1, Z_1, N_2, Z_2, R_{\text{cont}}, \beta_1, \beta_2, J) \end{aligned} \quad (5)$$

where $N = N_1 + N_2$ and $Z = Z_1 + Z_2$, and β_1 and β_2 represent quadrupole deformations of the two fragments, respectively. That the nucleon transfer process takes place can be assumed by $R_{\text{cont}} = R_1[1 + \beta_1 Y_{20}(\theta_1)] + R_2[1 + \beta_2 Y_{20}(\theta_2)] + 0.5$ fm, with $R_i = 1.16A_i^{1/3}$. $B(N_1, Z_1, \beta_1)$ and $B(N_2, Z_2, \beta_2)$ are the binding energies of two deformed nuclei, respectively. The deformation dependent binding energy is calculated by the macroscopic-microscopic model [57]. The nucleus-nucleus interaction potential energy $V_{\text{CN}}(N_1, Z_1, N_2, Z_2, R_{\text{cont}}, \beta_1, \beta_2)$ between two interacting nuclei of the DNS configuration is the sum of the nuclear interaction potential V_N obtained from the folding integral of a zero-range nucleon-nucleon interaction [58,59] and Coulomb interaction potential V_C calculated by Wong's formula [60]. The rotational energy $V_{\text{rot}} = \hbar^2 J(J+1)/I_{\text{tot}}$, where the moment of inertia I_{tot} is approximated by its rigid-body value.

To obtain the distribution isotopes of final products $\sigma_{Z_1, N_1}^{\text{fin}}(E_{\text{c.m.}})$, statistical model code GEMINI++ is employed. Here, one assumes that the sharing of the total excitation energy between the targetlike and projectilelike fragments is proportional to their masses $E_{Z_1, N_1}^* = E_{\text{tot}} \times A_1/(A_1 + A_2)$, where A_1 and A_2 are the corresponding mass numbers. Subsequent deexcitation cascades of the excited fragments via emission of light particles (neutron, proton, and α) and γ rays competing with the fission process are taken into account, which lead to the final mass distribution of the reaction products [61,62].

For a certain primary product, the deexcitation process should be simulated many times due to the statistical nature of GEMINI++. In the present paper, results obtained with $M_{\text{trial}} = 1000$ are presented. After M_{trial} times Monte Carlo simulations, events with (Z_1, N_1) are counted, and the number of such events is marked as $M(Z_1, N_1; Z'_1, N'_1, J')$. Then the decay probability from the primary product (Z'_1, N'_1, J') produced at the incident angular momentum J' to the final product (Z_1, N_1) can be estimated as $P(Z_1, N_1; Z'_1, N'_1, J') = M(Z_1, N_1; Z'_1, N'_1, J')/M_{\text{trial}}$ [53]. Finally, the production cross section of final product (Z_1, N_1) can be expressed as

$$\sigma_{Z_1, N_1}^{\text{fin}}(E_{\text{c.m.}}) = \sum_{Z'_1, N'_1, J'} \sigma_{\text{pri}}(Z'_1, N'_1, J') \times P(Z_1, N_1; Z'_1, N'_1, J'). \quad (6)$$

The details of GEMINI++ are given in Refs. [61,62].

III. RESULTS

A. Production cross sections of transuranium isotopes with $^{238}\text{U} + ^{238}\text{U}$ and $^{238}\text{U} + ^{248}\text{Cm}$ reactions

As mentioned in the Introduction, pioneering experiments using deeply inelastic reactions between very heavy nuclei, $^{238}\text{U} + ^{238}\text{U}$ and $^{238}\text{U} + ^{248}\text{Cm}$, have been carried out to determine the feasibility of using multinucleon transfer for production of superheavy nuclei. To test the predicted abilities of the production cross sections of these reactions within the improved DNS model + GEMINI++, the production cross sections of isotopes in the multinucleon transfer reactions $^{238}\text{U} + ^{238}\text{U}$ at bombarding energy $E_{\text{c.m.}} = 892.5$ MeV are calculated. Comparison of the experimental data with the calculated cross sections of transuranium nuclei is shown in Fig. 1. Here the experimental data are denoted by solid squares. The black solid lines denote the calculated results of the final products by using the improved DNS model + GEMINI++. It can be seen from Fig. 1 that a good agreement between the calculated results and the experimental data is shown.

One can see that the measured final isotopic yields of TLFs in the reaction $^{238}\text{U} + ^{238}\text{U}$ decrease drastically with increasing atomic number. The results of our calculations also drop exponentially with increasing atomic numbers of the final products; the theoretical production cross sections shown in Fig. 1 are in agreement with the changing trend of experimental data. One finds that the cross sections of the $^{238}\text{U} + ^{238}\text{U}$ reaction decrease drastically by a factor of 10 per proton, which is moved from projectile to target.

The present results of the $^{238}\text{U} + ^{238}\text{U}$ reaction are compared with the predictions of other groups. Systematic calculations have been made by Saiko and Karpov [21] to describe the multinucleon transfer cross sections in $^{238}\text{U} + ^{238}\text{U}$ and $^{238}\text{U} + ^{248}\text{Cm}$ reactions with the improved multidimensional Langevin-type dynamical approach. The calculated production cross section by Saiko and Karpov for the $^{238}\text{U} + ^{238}\text{U}$ reaction at the same $E_{\text{c.m.}} = 892.5$ MeV is denoted by blue dashed lines in Fig. 1; their results show that the magnitude and maxima of the observed TLF transfer cross sections ($\Delta Z = +2$ to $\Delta Z = +5$) can be reasonably described. However, for $\Delta Z = +6$ and $+8$, the theoretical results systematically underestimate the experimental production cross sections.

One can see that the calculated distribution of final fragments is obviously staggering in Fig. 1(g). This is due to odd-even effects and shell effects included in the ground state binding energy in Eq. (5). In principle, on the one hand, the shell damping is due to excitation energy converted from incident energy. Therefore, the temperature dependent binding energy should be considered [52]. On the other hand, the pairing correction energy should be excluded for calculating the level density in Fermi-gas-type models; the reason is addressed in detail in Ref. [63]. Thus, I also calculated the theoretical results in the case of the exclusion of pairing correction energy and including shell damping in the potential energy surface when determining the local excitation energy, as shown in Fig. 2. It can be seen that the calculated production cross sections with shell damping and without

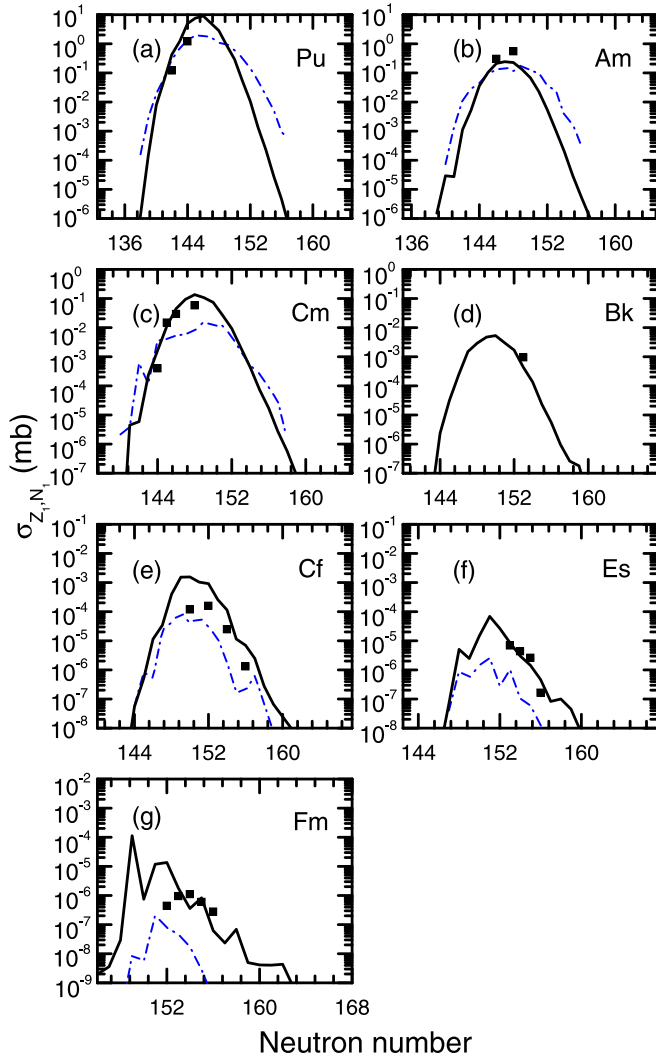


FIG. 1. The experimental production cross sections [6] compared to the calculated results for the $^{238}\text{U} + ^{238}\text{U}$ reaction at incident energy $E_{c.m.} = 892.5$ MeV. The calculated results using the improved DNS model + GEMINI++ are shown by solid lines. The blue dash-dotted lines denote the distributions of final fragments obtained from the improved multidimensional Langevin-type dynamical approach combined with the statistical model.

considering the pairing energy obviously change large jumps of theoretical results. In addition, weak odd-even effects still can be observed in the distribution of final fragments in Fig. 2 due to ground state binding energies which have been used to calculate neutron separation energies in the deexcitation processes.

In order to further test our model, the theoretical cross sections for the production of heavy actinides in damped collisions $^{238}\text{U} + ^{248}\text{Cm}$ at $E_{c.m.} = 898.7$ MeV are shown in Fig. 3. The experimental data of Ref. [7] are plotted as solid squares, and the calculated results are denoted by black solid lines. At first glance, there is a good agreement between theoretical and experimental cross sections for production of isotopes of the elements Bk, Cf, Es, Fm, and Md. If one looks carefully, however, there are deviations between theoretical and

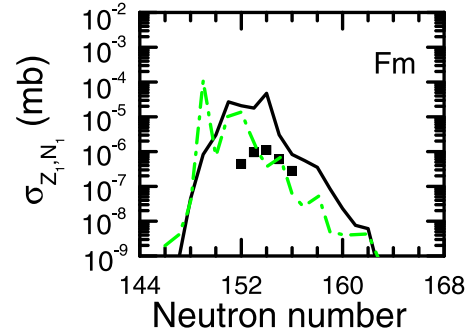


FIG. 2. Same as Fig. 1, the calculation of final products by using the improved DNS model + GEMINI++ with and without the exclusion of pairing correction energy and including shell damping in the potential energy surface, shown by black solid lines and blue dash-dotted lines, respectively.

experimental data. One can see a small shift of the maxima of the calculated distributions toward lower masses for the Fm and Md isotopes. Similar to the $^{238}\text{U} + ^{238}\text{U}$ reaction, the cross sections in the production of heavy targetlike fragments decrease drastically with the atomic numbers of the fragments.

Calculations of this reaction at the same incident energy $E_{c.m.} = 898.7$ MeV are performed by Saiko and Karpov [21] based on the improved multidimensional Langevin-type dynamical approach; the results are shown in Fig. 3 by blue dash-dotted lines. It can be seen from Fig. 3 that the production cross sections of the neutron-rich isotopes can be well reproduced by the improved multidimensional Langevin-type dynamical approach and a small shift of the maxima of the calculated distributions toward lower masses can be seen in Fig. 3 for the heaviest measured nuclides. In addition, the results of GRAZING-F are shown in Fig. 3 by red dashed lines for comparison [46]. The experimental data are compared with predictions using GRAZING-F; it is found that the GRAZING-F model is adequate for describing the magnitudes of the transfer cross sections for $+1p$, $+2p$, and $+3p$ transfers, whereas the calculated result is less successful for larger p transfer channels.

B. Comparison of the production cross sections from ^{136}Xe and ^{238}U projectiles bombarding the ^{248}Cm target

The calculated production cross sections of isotopes in the multinucleon transfer reactions $^{136}\text{Xe} + ^{248}\text{Cm}$ at bombarding energy $E_{c.m.} = 519.9$ MeV are shown in Fig. 4. The change of the proton number of the TLF from ^{248}Cm as a function of the neutron number of the TLF is denoted by black solid lines in Fig. 4. The experimental data are denoted by solid squares [11]. One can see from each panel of Fig. 4 that the production cross sections of one ($-1p$) to three proton ($-3p$) stripping channels are reproduced reasonably, and the theoretical cross sections in the TLF transfer product distributions using our model also agree with the observed maxima for $+1p$ to $+4p$ proton pick up channels. One also notices that the production cross sections of the above-target products for the $^{136}\text{Xe} + ^{248}\text{Cm}$ reaction decrease drastically by a factor of 10 per proton, which is moved from projectile to target.

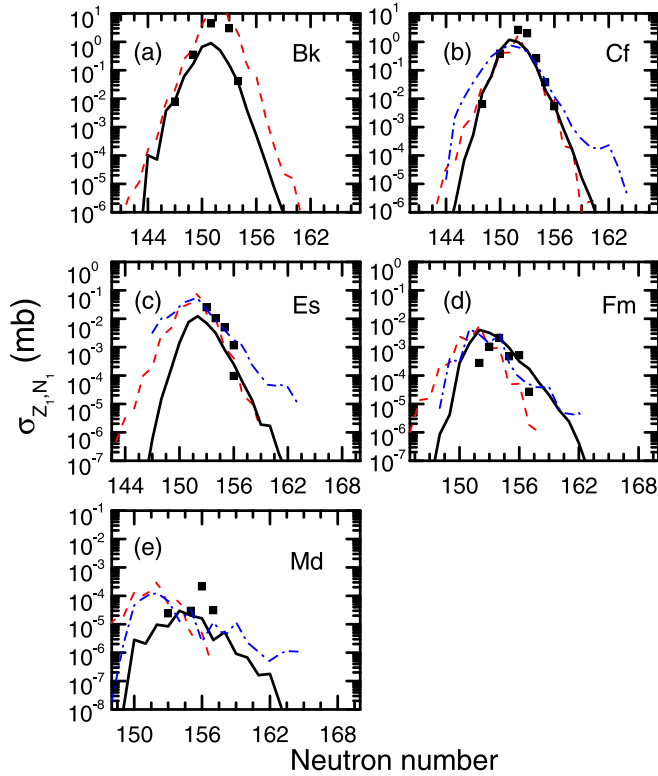


FIG. 3. The experimental production cross sections [7] compared to the calculated results for the $^{238}\text{U} + ^{248}\text{Cm}$ reaction at incident energy $E_{c.m.} = 898.7$ MeV. The calculated results using the improved DNS model + GEMINI++ are shown by solid lines. The red dashed lines and blue dash-dotted lines denote the distributions of final fragments obtained from GRAZING-F and the improved multi-dimensional Langevin-type dynamical approach combined with the statistical model, respectively.

One notices that the maxima of the calculated distributions of final fragments are shifted toward lower masses in Figs. 4(g) and 4(h). I also calculated the theoretical results in the case of the exclusion of pairing energy and including shell damping in the potential energy surface when determining the local excitation energy, as shown in Fig. 5. One can see that the calculated production cross section (black solid lines) with shell damping and without considering the pairing energy obviously agrees better with the experimental data for production of Es and Fm isotopes as compared in Figs. 4(g) and 4(h) (green dash-dotted lines).

The prediction of final products by using GRAZING-F is shown in Fig. 4 by red dashed lines for comparison. One can see that GRAZING-F seems to do a fair job in predicting the cross sections from $-1p$ to $+2p$ transfer channels but fails to reproduce the data for larger p transfers and some below-target yields.

Comparison of the production cross sections from different projectiles bombarding the same target through the multinucleon transfer reaction has aroused great interest in experimental and theoretical research. Therefore, in Fig. 4, I also compared the calculated Bk, Cf, Es, and Fm isotope distributions with the experimental values obtained from

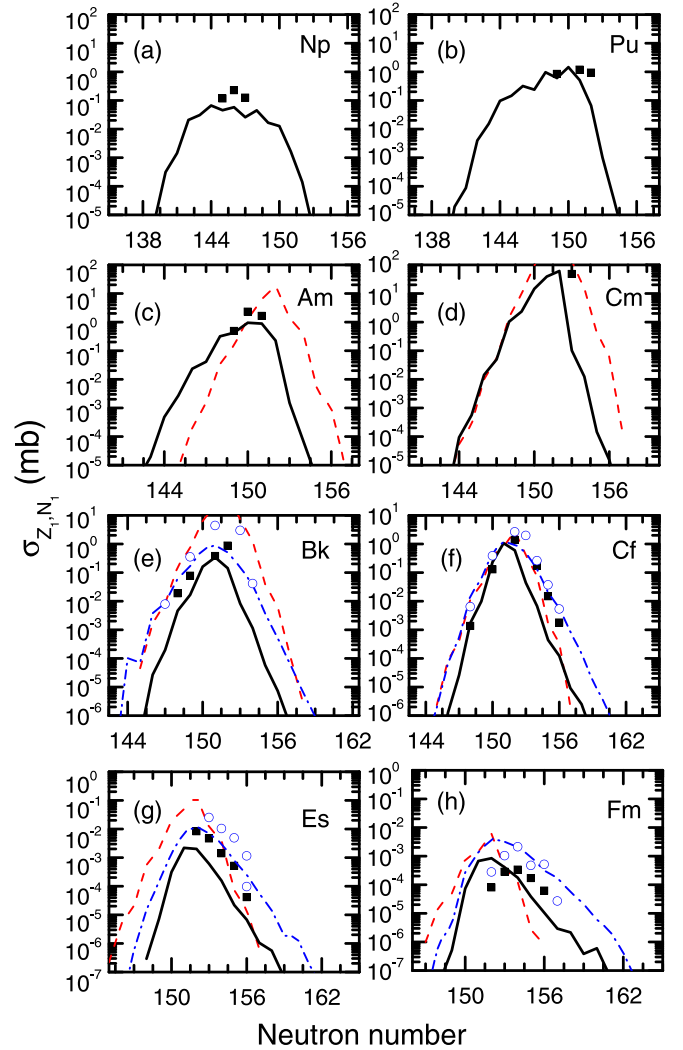


FIG. 4. The experimental production cross sections [7] compared to the calculated results for the $^{136}\text{Xe} + ^{248}\text{Cm}$ reaction at incident energy $E_{c.m.} = 519.9$ MeV. The calculated results using the improved DNS model + GEMINI++ are shown by solid lines. The red dashed lines denote the distributions of final fragments obtained from GRAZING-F for comparison. The experimental data of $^{238}\text{U} + ^{248}\text{Cm}$ reaction are denoted by blue open circles, and the calculation of final products by using the improved DNS model + GEMINI++ is shown by blue dash-dotted lines.

$^{136}\text{Xe} + ^{248}\text{Cm}$ and $^{238}\text{U} + ^{248}\text{Cm}$ reactions. The experimental data of the $^{238}\text{U} + ^{248}\text{Cm}$ reaction are denoted by blue open circles, and the calculation of final products using the improved DNS model + GEMINI++ is shown in Fig. 4 by blue dash-dotted lines. One finds that the distribution from the ^{238}U ($N/Z = 1.58$) induced reaction appears to extend out to larger neutron numbers than the ^{136}Xe ($N/Z = 1.51$) induced reaction. In addition, the results also showed that the absolute production cross sections of neutron-rich Bk, Cf, Es, and Fm isotopes increase for the ^{238}U induced reaction. The more neutron-rich and heavy ^{238}U projectile gives a TLF distribution that peaks at a larger neutron number for Bk, Cf, Es, and Fm isotopes compared to the ^{136}Xe projectile.

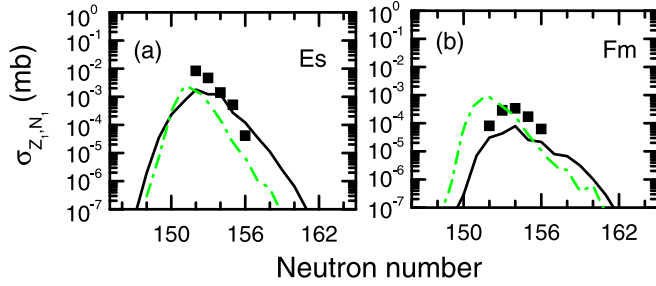


FIG. 5. Same as Fig. 4, the calculation of final products by using the improved DNS model + GEMINI++ with and without the exclusion of pairing correction energy and including shell damping in the potential energy surface, shown by black solid lines and blue dash-dotted lines, respectively.

In Fig. 6 the mass distributions of heavy primary and final products are shown for ^{238}U and ^{136}Xe with the ^{248}Cm target. One can see from Fig. 6(b) that the final mass distribution width increases with increasing projectile mass number for nuclei with production mass number more than 208, and the observation of relatively high yields of neutron-rich products with the ^{238}U induced reaction is encouraging for production of new neutron-rich heavy nuclei. The reason for this discrepancy corresponds to the usual quasifission process

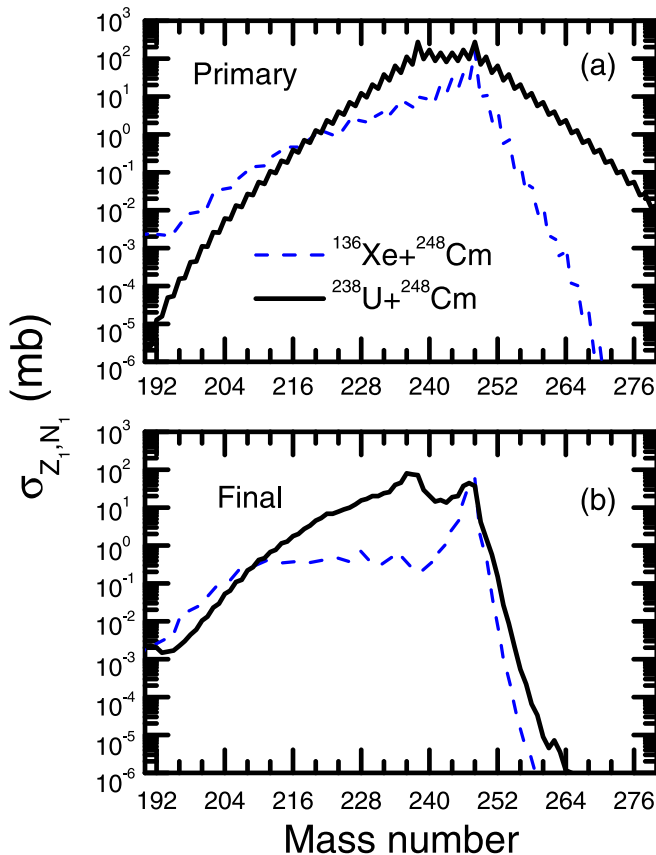


FIG. 6. Mass distributions of final products in the $^{136}\text{Xe} + ^{248}\text{Cm}$ reaction with bombarding energy $E_{c.m.} = 519.9$ MeV and $^{238}\text{U} + ^{248}\text{Cm}$ reaction with $E_{c.m.} = 898.7$ MeV.

(multinucleon rearrangement between primary fragments) in which nucleons are transferred mainly from the heavy target to the lighter projectile for the $^{136}\text{Xe} + ^{248}\text{Cm}$ reaction. However, in inverse quasifission the mass asymmetry is larger than the initial one for the $^{238}\text{U} + ^{248}\text{Cm}$ reaction because of the lead shoulder in the mass and charge distributions of the reaction fragments. As a result the cross sections for formation of new primary neutron-rich isotopes of transfermium elements in Fig. 6(a) in transfer reactions with the ^{248}Cm target are larger in reactions with a uranium beam as compared with the ^{136}Xe projectile.

C. The selection of the heaviest available target for the largest production cross sections for the given Z

The experimental production cross sections of heavy TLFs for the given Z are approximately two to three orders of magnitude larger for the $^{238}\text{U} + ^{248}\text{Cm}$ reaction as compared to the $^{238}\text{U} + ^{238}\text{U}$ reaction. This certainly motivates one to select the heaviest available target in order to achieve the largest production cross sections for heavy and superheavy nuclei in multinucleon transfer reactions. Therefore, we also predicted the production cross sections of isotopes in the multinucleon transfer reactions $^{136}\text{Xe} + ^{249}\text{Cf}$ at the incident energy $E_{c.m.} = 525.8$ MeV.

The experimental cross sections [64] according to the change of the proton number of the TLF from ^{249}Cf as functions of the neutron number of the TLF are shown in Fig. 7 by black squares. The calculated results using the improved DNS model + GEMINI++ are shown by green dash-dotted lines. At first glance, one can see from each panel of Fig. 7 that the agreement of the calculated results with the experimental data is reasonable good. One can see that the production cross sections of the above-target products for the $^{136}\text{Xe} + ^{249}\text{Cf}$ reaction decrease drastically by a factor of 10 per proton, which is moved from projectile to target. In addition, one notices that the experimental production cross sections of heavy TLFs for the given Z are approximately one to two orders of magnitude larger for the $^{136}\text{Xe} + ^{249}\text{Cf}$ reaction as compared to the $^{136}\text{Xe} + ^{248}\text{Cm}$ reaction.

Careful comparison of the measured cross sections with the calculated results reveals that the theoretical values systematically underestimate the experimental cross sections and shift left for odd p transfer channels (Bk, Es, and Md). Thus, I also predicted the theoretical results in the case of the exclusion of pairing energy and including shell damping in the potential energy surface when determining the local excitation energy, and the theoretical production cross section with shell damping and without pairing energy in the local excitation energy is shown by black solid lines in Fig. 7. It can be seen that the calculated production cross section (black solid lines) agrees better with the experimental data for production of Bk, Es, and Md isotopes. However, for Fm isotopes, the maxima of the calculated distributions of final fragments are reduced due to shell damping for the $N = 152$ neutron shell. Similar situations are also shown in Fig. 5(b).

The predicted results using GRAZING-F at $E_{c.m.} = 525.8$ MeV are shown in Fig. 7 for comparison. It can be seen that the final mass distribution obtained from

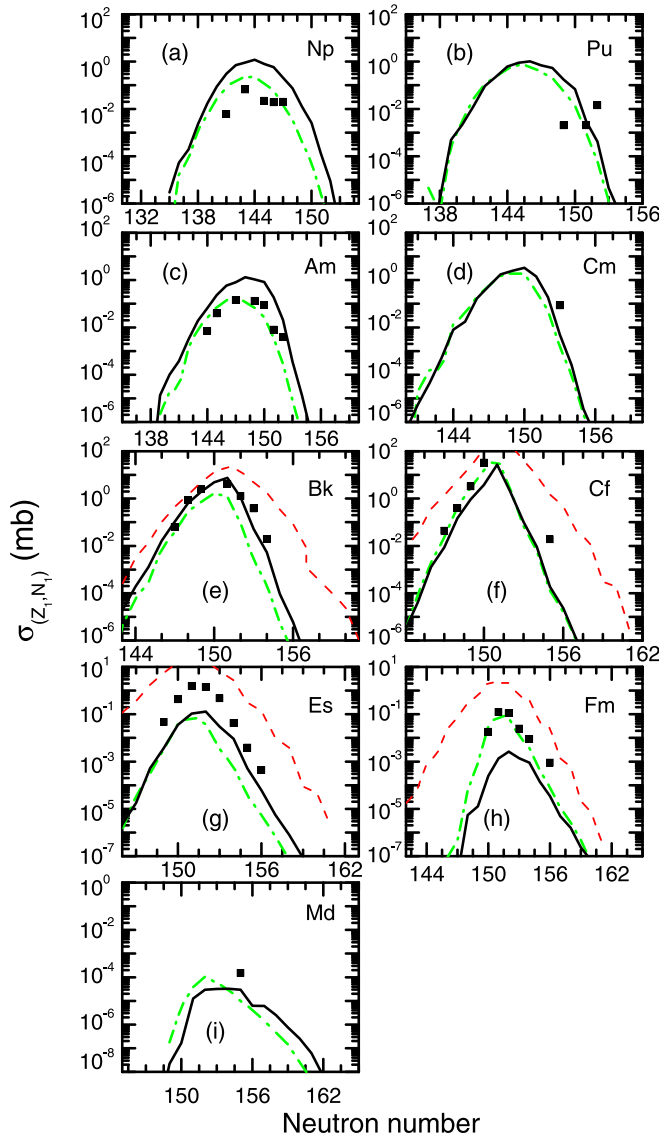


FIG. 7. The experimental production cross sections [7] compared to the calculated results for the $^{136}\text{Xe} + ^{249}\text{Cf}$ reaction at incident energy $E_{\text{c.m.}} = 525.8$ MeV. The calculated results using the improved DNS model + GEMINI++ are shown by solid lines. The calculations of final products by using the improved DNS model + GEMINI++ with and without the exclusion of pairing correction energy and including shell damping in the potential energy surface are shown by black solid lines and blue dash-dotted lines, respectively. The red dashed lines denote the distributions of final fragments obtained from GRAZING-F for comparison.

GRAZING-F seems to predict the location of the maximum of the mass yields but fails to predict the absolute values, overestimating the cross sections by an order of magnitude.

D. Prediction of new transfermium isotopes

The above results give us opportunities and challenges to investigate the multinucleon transfer reactions leading to new transfermium isotopes by collisions between very heavy nuclei. The opportunity lies in using the heaviest available target

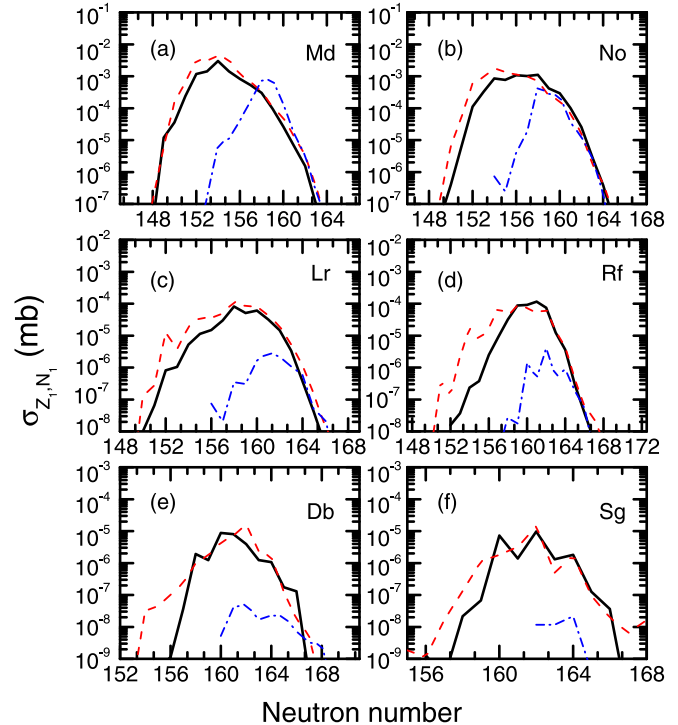


FIG. 8. Predicted targetlike production cross sections of ^{238}U , ^{248}Cm , and $^{144}\text{Xe} + ^{249}\text{Cf}$ reactions are represented by solid lines, red dashed lines, and blue dash-dotted lines, respectively.

to produce the largest cross sections for new transfermium isotopes. Therefore, the other combinations of actinide projectiles and targets can also be considered for future experiments on the production of new transfermium nuclei. The challenges come from an exponential drop in the isotopic distributions of the above-target products formed in the collisions of actinides with an increasing atomic number. In addition, it is very difficult to perform such experiments especially with actinide targets because of the high fission probability of excited heavy reaction products.

In Fig. 8 the predicted cross sections are shown for the production of final fragments in damped collisions with three different projectiles bombarding the same ^{249}Cf target. The predicted results using the improved DNS model + GEMINI++ are shown for $^{238}\text{U} + ^{249}\text{Cf}$ and $^{248}\text{Cm} + ^{249}\text{Cf}$ reactions by solid lines and red dashed lines, respectively. The blue dash-dotted lines denote the distributions of final fragments obtained from the $^{144}\text{Xe} + ^{249}\text{Cf}$ reaction for comparison. One finds that the $^{144}\text{Xe} + ^{249}\text{Cf}$ reaction has no advantage for production of new transfermium isotopes due to the very low beam intensity of ^{144}Xe . There is a gap between the transfermium synthesized by cold fusion and that synthesized by hot fusion [65]. The calculated results show that large cross sections ($\sigma_{1n} \geq 1$ pb) for many transfer channels can be used to fill the gap and produce neutron-rich transfermium nuclei.

In Fig. 8, the predicted production cross section for the reaction $^{248}\text{Cm} + ^{249}\text{Cf}$ is given. The transfer cross sections of ^{261}Md and ^{262}Md are 49.8 and 12.6 pb, respectively. It is 3.4 pb for ^{263}Md . The predicted cross sections of ^{261}No ,

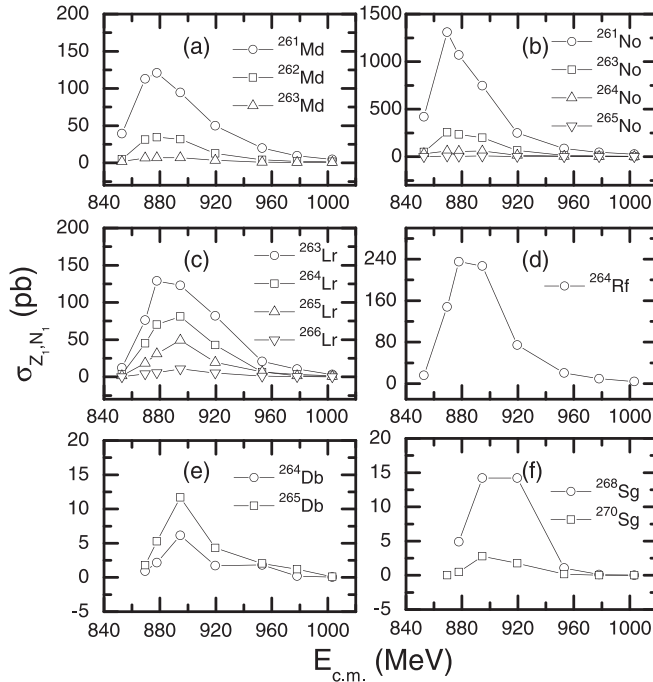


FIG. 9. Excitation functions for the production of new transfermium isotopes $^{261,262}\text{Md}$, $^{261,263-265}\text{No}$, $^{263-266}\text{Lr}$, ^{264}Rf , $^{264,265}\text{Db}$, and $^{268,270}\text{Sg}$ in the $^{248}\text{Cm} + ^{249}\text{Cf}$ reaction.

^{263}No , ^{264}No , and ^{265}No are 249.3, 66.5, 16.1, and 1.8 pb, respectively. The calculated transfer cross sections of ^{263}Lr , ^{264}Lr , ^{265}Lr , and ^{266}Lr are 81.9, 42.7, 19.6, and 5.18 pb, respectively. The predicted transfer cross section of the ^{264}Rf is 74.3 pb. The transfer cross sections of ^{264}Db and ^{265}Db are 1.72 and 4.32 pb, respectively. The transfer cross sections of ^{268}Sg and ^{270}Sg are 14.2 and 1.77 pb, respectively. Through the analysis of Figs. 8(a)–8(f), I found that nuclei $^{261,262}\text{Md}$, $^{261,263-265}\text{No}$, $^{263-266}\text{Lr}$, ^{264}Rf , $^{264,265}\text{Db}$, and $^{268,270}\text{Sg}$ may be produced. In some cases the yields of as yet unknown neutron-enriched isotopes of heavy actinides are sufficiently large for their experimental identification. In addition, one finds that the production of the surviving heavy fragments with the charged number $Z > 106$ is rare because of the very small cross sections at the level of 1 pb and even below 1 pb.

The final cross section is a product of the primary cross section and survival probability. With increasing beam energy the yield of primary fragments increases. However the excitation energy of these fragments also increases and thus decreases their survival probabilities. Therefore, determination of an optimal collision energy is of great importance for planning experiments on production of new transfermium isotopes.

The production cross sections for $^{261,262,263}\text{Md}$, $^{261,263-265}\text{No}$, $^{263-266}\text{Lr}$, ^{264}Rf , $^{264,265}\text{Db}$, and $^{268,270}\text{Sg}$ isotopes are shown in Fig. 9 for $^{248}\text{Cm} + ^{249}\text{Cf}$ collisions at different beam energies. We may conclude that the optimal beam energy for the production of new transfermium isotopes in multinucleon transfer reactions with heavy actinide nuclei is very close to the energy needed for these nuclei to reach the contact configuration ($\approx 1.05V_{\text{Bass}}$). The excitation function for the production of a given isotope of transfermium isotopes in the transfer reaction is much wider as compared to the fusion excitation functions.

IV. SUMMARY

The multinucleon transfer processes in low energy heavy-ion collisions have been analyzed by considering the influence of the orientation effects using the improved DNS model combined with GEMINI++. The developed approach allows us to calculate the production cross sections of the above-target fragments in collisions of heavy actinides at near-barrier collision energies. The calculated results are in good agreement with experimental data for $^{238}\text{U} + ^{238}\text{U}$, ^{248}Cm and $^{136}\text{Xe} + ^{248}\text{Cm}$, ^{249}Cf reactions. Because of high excitation energies and angular momenta of the primary fragment, one finds that the theoretical and experimental production cross sections show a strong exponential drop with an increasing atomic number.

This trend makes the production of new superheavy isotopes hardly reachable using multinucleon transfer reactions. However, the experimental and theoretical production cross sections of heavy TLFs for the given Z are approximately two to three orders of magnitude larger for the $^{238}\text{U} + ^{248}\text{Cm}$ reaction as compared to $^{238}\text{U} + ^{238}\text{U}$ reaction, and the results for the given Z are approximately one to two orders of magnitude larger for the $^{136}\text{Xe} + ^{249}\text{Cf}$ reaction as compared to the $^{136}\text{Xe} + ^{248}\text{Cm}$ reaction. One finds that the heaviest available actinide target can be used to produce the new transfermium isotopes. Therefore, the possibility of producing new transfermium isotopes in the $^{238}\text{U} + ^{249}\text{Cf}$, $^{248}\text{Cm} + ^{249}\text{Cf}$, and $^{144}\text{Xe} + ^{249}\text{Cf}$ reactions has been predicted. The incident energy dependence of the production cross section of new transfermium isotopes in the $^{248}\text{Cm} + ^{249}\text{Cf}$ reaction has been calculated for determining the conditions for their synthesis. The predicted cross section for the yields of neutron-rich transfermium isotopes may be useful for the design of appropriate experimental equipment and for carrying out experiments of such kind.

ACKNOWLEDGMENT

This work is supported by the National Natural Science Foundation of China (Grant No. 11705055).

- [1] H. Freiesleben and J. V. Kratz, *Phys. Rep.* **106**, 1 (1984).
- [2] J. V. Kratz, W. Loveland, and K. J. Moody, *Nucl. Phys. A* **944**, 117 (2015).
- [3] L. Corradi, G. Pollarolo, and S. Szilner, *J. Phys. G* **36**, 113101 (2009).

- [4] F. S. Zhang, C. Li, L. Zhu, and P. W. Wen, *Front. Phys.* **13**, 132113 (2018).
- [5] W. D. Loveland, *Front. Phys.* **7**, 23 (2019).
- [6] M. Schädel, J. V. Kratz, H. Ahrens, W. Bröchle, G. Franz, H. Gäggeler, I. Warnecke, G. Wirth, G. Herrmann,

- N. Trautmann, and M. Weis, *Phys. Rev. Lett.* **41**, 469 (1978).
- [7] M. Schädel, W. Bröchle, H. Gäggeler, J. V. Kratz, K. Stümmerer, G. Wirth, G. Herrmann, R. Stakemann, G. Tittel, N. Trautmann *et al.*, *Phys. Rev. Lett.* **48**, 852 (1982).
- [8] A. G. Artukh, V. V. Avdeichikov, G. F. Gridnev, V. L. Mikheev, V. V. Volkov, and J. Wilczyński, *Nucl. Phys. A* **176**, 284 (1971).
- [9] D. Lee, K. J. Moody, M. J. Nurmia, G. T. Seaborg, H. R. von Gunten, and D. C. Hoffman, *Phys. Rev. C* **27**, 2656 (1983).
- [10] D. C. Hoffman, M. M. Fowler, W. R. Daniels, H. R. von Gunten, D. Lee, K. J. Moody, K. Gregorich, R. Welch, G. T. Seaborg, W. Bröchle *et al.*, *Phys. Rev. C* **31**, 1763 (1985).
- [11] K. J. Moody, D. Lee, R. B. Welch, K. E. Gregorich, G. T. Seaborg, R. W. Loughheed, and E. K. Hulet, *Phys. Rev. C* **33**, 1315 (1986).
- [12] A. Türler, H. R. von Gunten, J. D. Leyba, D. C. Hoffman, D. M. Lee, K. E. Gregorich, D. A. Bennett, R. M. Chasteler, C. M. Gannett, H. L. Hall *et al.*, *Phys. Rev. C* **46**, 1364 (1992).
- [13] V. I. Zagrebaev and Walter Greiner, *J. Phys. G* **34**, 2265 (2007).
- [14] G. G. Adamian, N. V. Antonenko, A. Diaz-Torres, and S. Heinz, *Eur. Phys. J. A* **56**, 47 (2020).
- [15] S. Hofmann and G. Münzenberg, *Rev. Mod. Phys.* **72**, 733 (2000).
- [16] S. A. Giuliani, Z. Matheson, W. Nazarewicz, E. Olsen, P.-G. Reinhard, J. Sadhukhan, B. Schuettrumpf, N. Schunck, and P. Schwerdtfeger, *Rev. Mod. Phys.* **91**, 011001 (2019).
- [17] V. I. Zagrebaev and W. Greiner, *Nucl. Phys. A* **944**, 257 (2015).
- [18] V. I. Zagrebaev and W. Greiner, *Phys. Rev. C* **87**, 034608 (2013).
- [19] A. Winther, *Nucl. Phys. A* **572**, 191 (1994); **594**, 203 (1995).
- [20] V. I. Zagrebaev and W. Greiner, *Phys. Rev. Lett.* **101**, 122701 (2008).
- [21] V. V. Saiko and A. V. Karpov, *Phys. Rev. C* **99**, 014613 (2019).
- [22] G. G. Adamian, N. V. Antonenko, and A. S. Zubov, *Phys. Rev. C* **71**, 034603 (2005).
- [23] G. G. Adamian, N. V. Antonenko, V. V. Sargsyan, and W. Scheid, *Phys. Rev. C* **81**, 024604 (2010).
- [24] K. Zhao, Z. Li, N. Wang, Y. Zhang, Q. Li, Y. Wang, and X. Wu, *Phys. Rev. C* **92**, 024613 (2015).
- [25] C. Li, F. Zhang, J. Li, L. Zhu, J. Tian, N. Wang, and F. S. Zhang, *Phys. Rev. C* **93**, 014618 (2016).
- [26] N. Wang and Lu Guo, *Phys. Lett. B* **760**, 236 (2016).
- [27] L. Zhu, Z. Q. Feng, and F. S. Zhang, *J. Phys. G* **42**, 085102 (2015).
- [28] L. Zhu, J. Su, W. J. Xie, and F. S. Zhang, *Phys. Rev. C* **94**, 054606 (2016).
- [29] Z. Q. Feng, *Phys. Rev. C* **95**, 024615 (2017).
- [30] L. Zhu, J. Su, W. J. Xie, and F. S. Zhang, *Phys. Lett. B* **767**, 437 (2017).
- [31] K. Sekizawa and K. Yabana, *Phys. Rev. C* **88**, 014614 (2013).
- [32] K. Sekizawa, *Phys. Rev. C* **96**, 041601(R) (2017).
- [33] K. Godbey, C. Simenel, and A. S. Umar, *Phys. Rev. C* **101**, 034602 (2020).
- [34] X. Jiang and N. Wang, *Phys. Rev. C* **101**, 014604 (2020).
- [35] L. Guo, C. Simenel, L. Shi, and C. Yu, *Phys. Lett. B* **782**, 401 (2018).
- [36] Z. J. Wu and L. Guo, *Phys. Rev. C* **100**, 014612 (2019).
- [37] Z. Q. Feng, G. M. Jin, and J. Q. Li, *Phys. Rev. C* **80**, 067601 (2009).
- [38] A. V. Karpov and V. V. Saiko, *Phys. Rev. C* **96**, 024618 (2017).
- [39] X. Jiang and N. Wang, *Front. Phys.* **8**, 38 (2020).
- [40] Y. E. Penionzhkevich, G. G. Adamian, and N. V. Antonenko, *Eur. Phys. J. A* **27**, 187 (2006).
- [41] S. Ayik, B. Yilmaz, O. Yilmaz, and A. S. Umar, *Phys. Rev. C* **100**, 014609 (2019).
- [42] S. Ayik, B. Yilmaz, O. Yilmaz, A. S. Umar, and G. Turan, *Phys. Rev. C* **96**, 024611 (2017).
- [43] S. Ayik, B. Yilmaz, O. Yilmaz, and A. S. Umar, *Phys. Rev. C* **97**, 054618 (2018).
- [44] X. Jiang and N. Wang, *Chin. Phys. C* **42**, 104105 (2018).
- [45] C. Li, C. A. T. Sokhna, X. Xu, J. Li, G. Zhang, B. Li, Z. Ge, and F.-S. Zhang, *Phys. Rev. C* **99**, 034619 (2019).
- [46] R. Yanez and W. Loveland, *Phys. Rev. C* **91**, 044608 (2015).
- [47] X. J. Bao, *Phys. Rev. C* **102**, 054613 (2020); **102**, 064604 (2020).
- [48] P. W. Wen, A. K. Nasirov, C. J. Lin, and H. M. Jia, *J. Phys. G* **47**, 075106 (2020).
- [49] X. J. Bao, S. Q. Guo, H. F. Zhang, and J. Q. Li, *Phys. Rev. C* **97**, 024617 (2018).
- [50] X. J. Bao, S. Q. Guo, H. F. Zhang, and J. Q. Li, *Phys. Lett. B* **785**, 221 (2018).
- [51] X. J. Bao, *Nucl. Phys. A* **986**, 60 (2019).
- [52] X. J. Bao, *Phys. Rev. C* **100**, 011601(R) (2019).
- [53] S. Q. Guo, X. J. Bao, H. F. Zhang, J. Q. Li, and N. Wang, *Phys. Rev. C* **100**, 054616 (2019).
- [54] G. Wolschin and W. Nörenberg, *Z. Phys. A* **284**, 209 (1978).
- [55] C. Riedel, G. Wolschin, and W. Norenberg, *Z. Phys. A* **290**, 47 (1979).
- [56] J. Q. Li and G. Wolschin, *Phys. Rev. C* **27**, 590 (1983).
- [57] N. Wang, M. Liu, and X. Wu, *Phys. Rev. C* **81**, 044322 (2010).
- [58] G. G. Adamian, N. V. Antonenko, R. V. Jolos, S. P. Ivanova, and O. I. Melnikova, *Int. J. Mod. Phys. E* **05**, 191 (1996).
- [59] Q. F. Li, W. Zuo, W. F. Li, N. Wang, E. G. Zhao, J. Q. Li, and W. Scheid, *Eur. Phys. J. A* **24**, 223 (2005).
- [60] C. Y. Wong, *Phys. Rev. Lett.* **31**, 766 (1973).
- [61] R. J. Charity, *Phys. Rev. C* **82**, 014610 (2010).
- [62] D. Mancusi, R. J. Charity, and J. Cugnon, *Phys. Rev. C* **82**, 044610 (2010).
- [63] T. Rauscher, F.-K. Thielemann, and K.-L. Kratz, *Phys. Rev. C* **56**, 1613 (1997).
- [64] K. E. Gregorich, K. J. Moody, D. Lee, W. K. Kot, R. B. Welch, P. A. Wilmarth, and G. T. Seaborg, *Phys. Rev. C* **35**, 2117 (1987).
- [65] S. Hofmann, *Radiochim. Acta* **99**, 405 (2011).